*BCSJ Award Article*

# Effects of Metal Doping on the Spin-Crossover Properties of an Iron(II) Complex with Extended π-Conjugated Schiff-Base Ligand Having an $N_4O_2$ Donor Set

**Zhong Yu, Takayoshi Kuroda-Sowa,* Hiroaki Kume, Takashi Okubo, Masahiko Maekawa, and Megumu Munakata**

Department of Chemistry, School of Science and Engineering, Kinki University, Higashi-Osaka, Osaka 577-8502

Received November 5, 2008; E-mail: kuroda@chem.kindai.ac.jp

The spin-crossover (SCO) complex $[Fe(qnal)_2]\cdot CH_2Cl_2$ (**1**), (Hqnal: *N*-(8′-quinolyl)-2-hydroxy-1-naphthaldimine) with an $N_4O_2$ donor set, has been synthesized and characterized. Investigation of magnetic properties shows that the complex exhibits an abrupt and complete spin transition with a 5 K wide thermal hysteresis loop. The X-ray diffraction analysis of complex **1** reveals that the molecules are connected into a quasi one-dimensional chain through extended π–π interactions between aromatic rings of ligands. The effects of metal doping on SCO properties have been investigated in the mixed-metal system $[Fe_{1-x}M_x(qnal)_2]\cdot CH_2Cl_2$ (M = zinc(II) and nickel(II)). The results reveal that metal doping increases the gradual character of spin transition, and no marked differences found between zinc and nickel doping, which suggest the dominant effect of the doping-degree (concentration) rather than metal species on cooperativity. However, the metal doping shows different effects on critical temperature ($T_{1/2}$), where a more pronounced descending of $T_{1/2}$ is observed in response to increased Zn-doping than in Ni-doping, indicating the noticeable consequence of internal pressure due to the different radii of doping metal ions.

Since the discovery of the first spin-crossover (SCO) compound,[1,2] such complexes have aroused more and more attention for potential applications in molecular switches or in data storage devices.[3–7] SCO is not only induced by external stimulus (temperature, pressure, light irradiation, or magnetic field) but is altered by internal constraints such as structural changes of molecules and crystal lattices. In the solid state, SCO behavior can be understood as an entropically driven phenomenon,[8] which is favored by large structural changes during the process. Because of the large change in metal–ligand bond lengths between the HS and LS states, iron(II)/N-ligand combinations have the possibility to induce large cooperative spin transition between spin centers.[9] Hence SCO is frequently observed in complexes containing iron(II) with an $N_6$ coordination sphere but rare for compounds with $N_4O_2$[10–13] or $N_4S_2$[14] donor sets.

In the solid state, spin transitions between LS and HS states depend strongly on cooperativity, which is sensitive to the coupling between the adjacent spin centers, metal–donor bond length, and the crystal lattice vibrations.[15] Hence, it is possible for these complexes to affect a spin transition in a certain range by variation of the intermolecular interaction of compounds. Metal doping is an available strategy to control and adjust these interactions. Although a number of studies have examined metal-doping behaviors in iron(II) complexes exhibiting thermal spin crossover,[16–24] few studies have investigated SCO iron(II) species with $N_4O_2$ donors.

In the present work, we investigate experimentally metal-doping effects on the SCO properties of $[Fe(qnal)_2]\cdot CH_2Cl_2$, which we reported previously as an iron(II) complex with an $N_4O_2$ donor set.[25] This complex exhibited completely thermally-induced SCO behavior and a well-shaped 5 K wide hysteresis loop. Zinc(II) and nickel(II) were selected as doping metal ions for comparative information. The magnetic measurements were performed on mixed crystalline samples of $[Fe_{1-x}M_x(qnal)_2]\cdot CH_2Cl_2$ in given $x$ fraction.

## Experimental

**General Procedure.** All chemicals and solvents were used as received. The solvents used for the synthesis of complexes were distilled prior to use. All preparations and manipulations were performed under argon atmosphere using Schlenk techniques. The ligand *N*-(8′-quinolyl)-2-hydroxy-1-naphthaldimine was synthesized by the condensation of 8-aminoquinoline and 2-hydroxy-1-naphthaldehyde in absolute methanol according to literature procedures.[26]

**Preparation of $[Fe(qnal)_2]\cdot CH_2Cl_2$ (1).** A solution of $Fe(BF_4)_2\cdot 6H_2O$ (0.05 mmol, 16.8 mg) and antioxidant L-(+)-ascorbic acid (0.05 mmol, 8.8 mg) in methanol (10 mL) was layered over a solution of Hqnal (0.1 mmol, 29.8 mg) in dichlo-

Published on the web March 12, 2009; doi:10.1246/bcsj.82.333

romethane (10 mL). Dark brown needle crystals of **1** suitable for X-ray diffraction were obtained after one week at room temperature. Anal. Calcd for $C_{41}H_{28}Cl_2FeN_4O_2$: C, 66.96; H, 3.84; N, 7.62%. Found: C, 66.14; H, 4.22; N, 7.70%.

**Preparation of Doped Compounds.** The samples of doped compounds $[Fe_{1-x}M_x(qnal)_2]\cdot CH_2Cl_2$ (M = zinc(II) and nickel(II)) were prepared according to the same procedure, replacing $Fe(BF_4)_2\cdot 6H_2O$ by a mixture of $FeSO_4\cdot 7H_2O$ and $ZnSO_4\cdot 7H_2O$ (or $NiSO_4\cdot 6H_2O$) in given ratios. Dark brown needle crystals of doped compounds were obtained after one week. Iron(II) and zinc(II) or nickel(II) fractions were calculated from their concentration determined by ICP analysis.

**Magnetic Susceptibility.** Direct current (dc) magnetic susceptibility data were collected on microcrystalline or single-crystal samples on a Quantum Design MPMS2 SQUID magnetometer equipped with a 1 T magnet and capable of achieving temperatures of 4 to 350 K. A diamagnetic correction to the observed susceptibilities was applied using Pascal's constants.

**X-ray Structure Analysis.** Diffraction data for $[Fe(qnal)_2]\cdot CH_2Cl_2$ was collected at 293.1 and 123.1 K on a Rigaku/MSC CCD area detector with a Rigaku AFC10 diffractometer equipped with graphite monochromated Mo K$\alpha$ radiation. The structure was solved by a direct method (SHELXS-97)[27] and expanded using Fourier techniques. The non-hydrogen atoms were refined either anisotropically or isotropically by full-matrix least-squares calculations (SHELXS-97). Hydrogen atoms were not included. Reliability factors are defined as $R_1 = \sum ||F_o| - |F_c|| / \sum |F_o|$ and $wR_2 = [\sum w(F_o^2 - F_c^2)^2 / \sum w(F_o^2)^2]^{1/2}$. The obtuse cell choice at 293.1 K is converted from the original acute set ($a = 11.988(2)$, $b = 12.631(2)$, $c = 13.289(2)$ Å, $\alpha = 64.94(2)°$, $\beta = 64.12(2)°$, $\gamma = 71.70(2)°$) for easy comparison to the 123.1 K data.

Crystallographic data have been deposited with the Cambridge Crystallographic Data Centre: Deposition number CCDC-282609 and -282610 for $[Fe(qnal)_2]\cdot CH_2Cl_2$ at 123.1 and 293.1 K respectively. Copies of the data can be obtained free of charge via http://www.ccdc.cam.ac.uk/conts/retrieving.html (or from the Cambridge Crystallographic Data Centre, 12, Union Road, Cambridge, CB2 1EZ, U.K.; Fax: +44 1223 336033; e-mail: deposit@ccdc.cam.ac.uk).

## Results and Discussion

X-ray structure analyses of complex **1** were performed at 123.1 and 293.1 K, where the iron(II) ions are in the LS and HS states, respectively. Table 1 summarizes the experimental crystal data at 123.1 and 293.1 K, and their selected bond lengths and bond angles are listed in Table 2. At both temperatures, the compound crystallized in the triclinic space group $P\bar{1}$ with a 3.2% increase in volume of the unit cell. In complex **1**, iron(II) ion is coordinated by a pair of planer NNO tridentate ligands in a meridional fashion, representing a distorted octahedron geometry (Figure 1a).

The average Fe–N distances of 1.943(4) Å at 123.1 K and 2.164(5) Å at 293.1 K correspond to the value expected for an iron(II) ion in the LS and HS states, respectively. The change of 0.22 Å for Fe–N distance represents a characteristic features of spin-crossover iron(II) complexes.[8] The average bond lengths of Fe–N and Fe–O are almost the same at 123.1 K, but a 0.148 Å difference was found at 293.1 K. All of the 12 angles subtended off the iron(II) center lie in a range from 83.4(2) to 95.2(2)° at 123.1 K and from 75.9(2) to 102.0(2)° at 293.1 K, while the bond angles of the three axes (O1–Fe1–N1, O2–Fe1–N3, and N2–Fe1–N4) are considerably deviated from the ideal octahedral 180° (Table 2).

**Table 1.** Crystallographic Data for $[Fe(qnal)_2]\cdot CH_2Cl_2$ at 123.1 K (LS) and 293.1 K (HS)

| | 123.1 K | 293.1 K |
|---|---|---|
| Formula | $C_{41}H_{28}Cl_2FeN_4O_2$ | $C_{41}H_{28}Cl_2FeN_4O_2$ |
| Formula weight | 733.43 | 733.43 |
| Crystal system | triclinic | triclinic |
| Space group | $P\bar{1}$ | $P\bar{1}$ |
| $T$/K | 123.1 | 293.1 |
| $a$/Å | 12.201(6) | 11.988(2) |
| $b$/Å | 12.550(6) | 12.631(2) |
| $c$/Å | 12.985(7) | 13.462(3) |
| $\alpha$/° | 98.064(3) | 97.96(2) |
| $\beta$/° | 116.469(8) | 117.36(2) |
| $\gamma$/° | 110.004(7) | 108.30(3) |
| $V$/Å$^3$ | 1568.1(14) | 1619.3(9) |
| $Z$ | 2 | 2 |
| $D_{calcd}$/g cm$^{-3}$ | 1.566 | 1.504 |
| $\lambda$/Å | 0.71070 | 0.71070 |
| $\mu$/mm$^{-1}$ | 0.701 | 0.676 |
| $R_1$[a], $wR_2$[b] | 0.0700, 0.1940 | 0.0730, 0.1830 |

a) $R_1 = \sum ||F_o| - |F_c|| / \sum |F_o|$. b) $wR_2 = [\sum w(F_o^2 - F_c^2)^2 / \sum w(F_o^2)^2]^{1/2}$.

**Table 2.** Selected Bond Lengths/Å and Angles/° for $[Fe(qnal)_2]\cdot CH_2Cl_2$ at 123.1 K (LS) and at 293.1 K (HS)

| | 123.1 K | 293.1 K |
|---|---|---|
| Fe(1)–O(1) | 1.945(4) | 2.013(5) |
| Fe(1)–O(2) | 1.939(4) | 2.018(4) |
| Fe(1)–N(1) | 1.955(4) | 2.197(6) |
| Fe(1)–N(2) | 1.934(3) | 2.142(4) |
| Fe(1)–N(3) | 1.950(5) | 2.180(5) |
| Fe(1)–N(4) | 1.934(3) | 2.138(4) |
| O(1)–Fe(1)–O(2) | 89.3(2) | 97.0(2) |
| O(1)–Fe(1)–N(1) | 176.0(1) | 161.1(1) |
| O(1)–Fe(1)–N(2) | 92.7(1) | 85.6(2) |
| O(1)–Fe(1)–N(3) | 89.5(2) | 90.5(2) |
| O(1)–Fe(1)–N(4) | 88.8(1) | 102.0(2) |
| O(2)–Fe(1)–N(1) | 91.3(2) | 91.0(2) |
| O(2)–Fe(1)–N(2) | 88.5(2) | 102.0(2) |
| O(2)–Fe(1)–N(3) | 176.1(1) | 161.1(2) |
| O(2)–Fe(1)–N(4) | 92.6(2) | 85.6(2) |
| N(1)–Fe(1)–N(2) | 83.4(2) | 76.1(2) |
| N(1)–Fe(1)–N(3) | 90.2(2) | 87.2(2) |
| N(1)–Fe(1)–N(4) | 95.1(2) | 95.6(2) |
| N(2)–Fe(1)–N(3) | 95.2(2) | 95.8(2) |
| N(2)–Fe(1)–N(4) | 178.1(2) | 168.7(2) |
| N(3)–Fe(1)–N(4) | 83.6(2) | 75.9(2) |

In complex **1**, the dihedral angles between the quinolyl and naphthyl rings on each ligand are found to be different. At 123.1 K, they are 1.69 and 12.08° (hereafter denoted as ligand A and B, respectively). A detailed inspection of crystal structures revealed such dihedral angles on ligand A and B were 2.75 and 10.24° at 293.1 K, respectively.

The extensive $\pi$–$\pi$ stacking interactions between quinolyl and naphthyl rings from neighboring entities form a one-

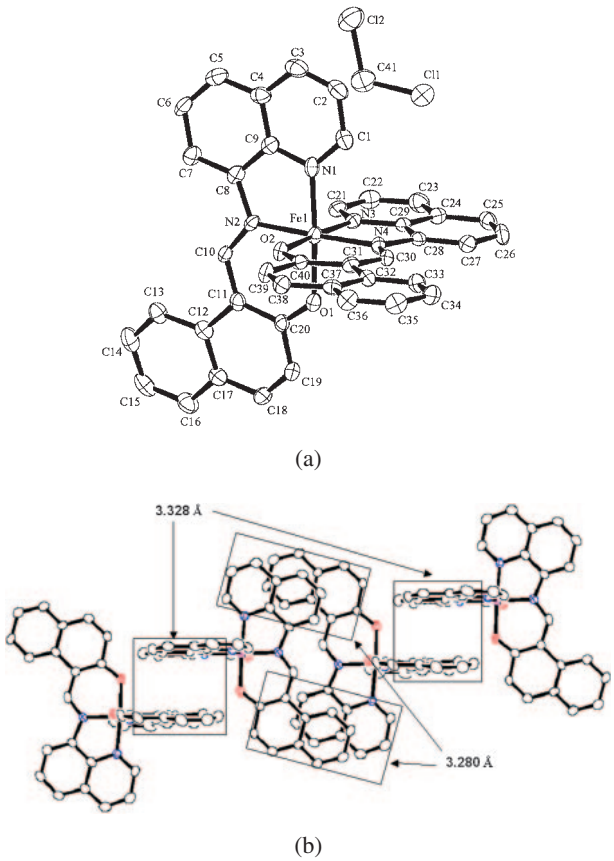


(a)

(b)

**Figure 1.** Molecular structures of $[Fe(qnal)_2]\cdot CH_2Cl_2$ in the LS state at 123.1 K. Hydrogen atoms are omitted for clarity. (a) ORTEP view showing 50% probability displacement ellipsoids. (b) One-dimensional structure assembled through $\pi$–$\pi$ interactions between quinolyl and naphthyl rings.

dimensional chain for complex **1** (Figure 1b). Dichloromethane solvent molecules are located in the lattice. Further analysis of the connectivity of the $\pi$–$\pi$ interaction indicates that complex **1** shows a structure with $\cdots$[A:Fe:B][B:Fe:A][A:Fe:B]$\cdots$, where [A:Fe:B] represents one molecule. It was found that ligand A always interacts with the neighboring ligand A (denoted A$\cdots$A) and vice versa for ligand B (denoted B$\cdots$B), and there is a difference in interactions between A$\cdots$A and B$\cdots$B. In the LS state, a shorter contact (shortest C–C distance = 3.280 Å) is observed at B$\cdots$B while a longer contact (3.328 Å) is observed at A$\cdots$A. Similar structural characteristics were observed in $[Fe^{III}(qsal)_2]$NCE (E = S and Se), where the complexes were treated as a dimer.[28] In this context, the combination of {[A:Fe:B][B:Fe:A]} can be regarded as a dimer in the LS state. It is however interesting to see in the HS state the shorter contact (3.356 Å) occurs at A$\cdots$A while a longer contact (3.380 Å) occurs at B$\cdots$B, i.e., {[B:Fe:A][A:Fe:B]}. This means that a switch of the dimer combination takes place in the lattice during spin transition. In this case, it is not suitable to treat complex **1** as a dimer. Such switching is probably induced by deformation of ligands, which suggests the sensitivity of the crystal lattice to different stretching of the ligand plane induced by the different occupancies of the antibonding $e_g$ orbitals on the center iron(II) ion accompanying the

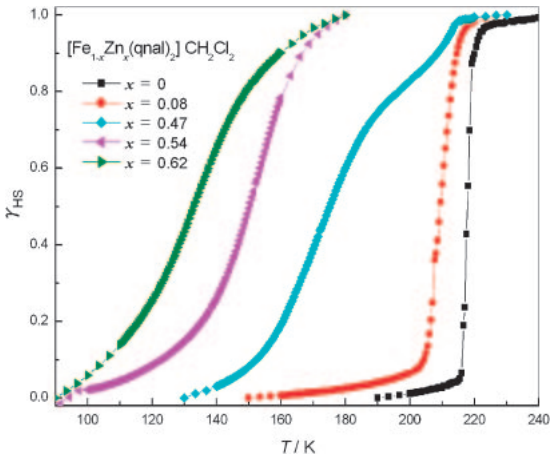


(a)

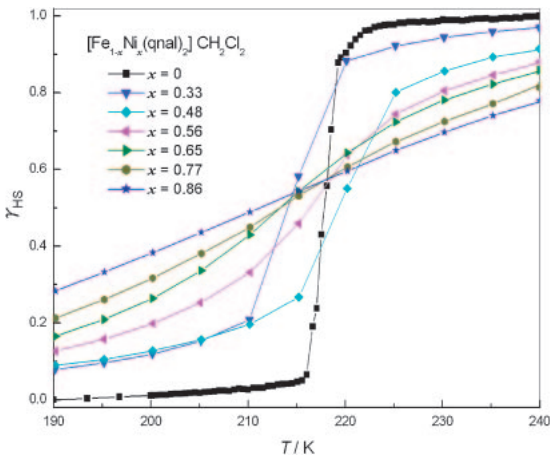


(b)

**Figure 2.** $\gamma_{HS}$ vs. $T$ curves for $[Fe_{1-x}Zn_x(qnal)_2]\cdot CH_2Cl_2$ (a) and $[Fe_{1-x}Ni_x(qnal)_2]\cdot CH_2Cl_2$ (b) in the region of the spin-transition.

spin transition between LS and HS states.

The doped complexes $[Fe_{1-x}M_x(qnal)_2]\cdot CH_2Cl_2$ were obtained as dark brown needle crystals from the reaction mixture of iron(II) sulfate and zinc(II) or nickel(II) sulfate with a given ratio in methanol, in which a dichloromethane solution of Hqnal ligand was added. The magnetic measurements were performed on crystalline samples of $[Fe_{1-x}Zn_x(qnal)_2]\cdot CH_2Cl_2$ (with $x = 0$, 0.08, 0.47, 0.54, and 0.62) and $[Fe_{1-x}Ni_x(qnal)_2]\cdot CH_2Cl_2$ (with $x = 0$, 0.33, 0.48, 0.56, 0.65, 0.77, and 0.86). Consideration of the spin magnetic moment of nickel(II) ($S = 1$) allows an understanding of the additional magnetic susceptibility disturbance induced by the nickel component in mixed-metal samples. To avoid this disturbance, we plotted HS molar fraction ($\gamma_{HS}$) as a function of $x$ for mixed-metal systems $[Fe_{1-x}M_x(qnal)_2]\cdot CH_2Cl_2$ (M = zinc(II) and nickel(II)) (Figure 2). The $\gamma_{HS}$ is calculated from the relationship $\gamma_{HS} = [\chi_m T - \chi_m T\ (LT)]/[\chi_m T\ (HT) - \chi_m T\ (LT)]$, where $\chi_m$ is the molar magnetic susceptibility, $\chi_m T\ (HT)/(LT)$ is the $\chi_m T$ value at the high/low-temperature limit, and $T$ the temperature.

As shown in Figure 2, pure $[Fe(qnal)_2]\cdot CH_2Cl_2$ sample exhibits an abrupt and complete spin transition at 217 K. As $x$ increases, the spin transition is found to become more gradual

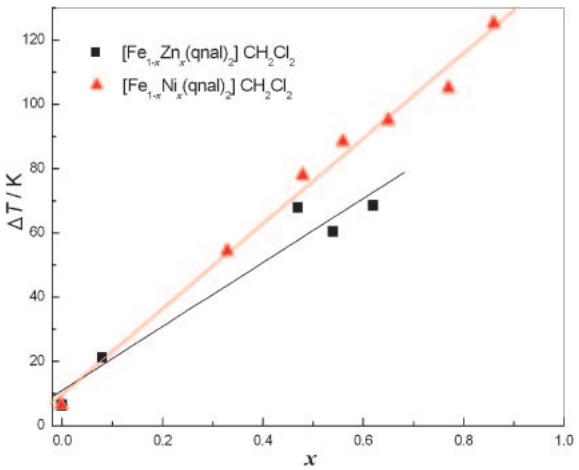


**Figure 3.** Evolution of $\Delta T$ as a function of $x$ fraction in doped species (Lines represent linear fit of the experimental data.).

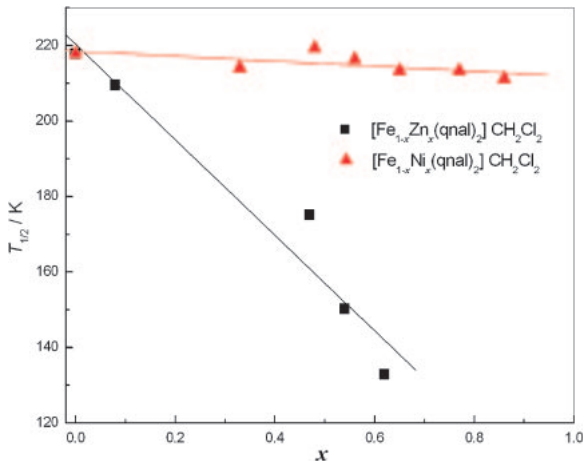


**Figure 4.** Evolution of the critical temperature $T_{1/2}$ as a function of $x$ fraction in doped species (Lines represent linear fit of the experimental data.).

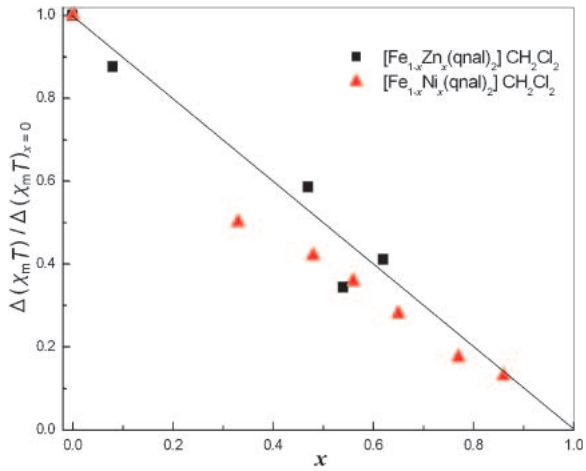


**Figure 5.** Evolution of the $\Delta(\chi_m T)/\Delta(\chi_m T)_{x=0}$ as a function of $x$ fraction in doped species.

in both cases. It is known that cooperative interactions derive from electron–phonon coupling between molecules. The involved foreign metal ions weaken the long-range elastic interactions between the SCO iron centers and further bring on the loss of cooperativity. In Figure 2, the gradual curves reflect the trend of this loss with increased doping, i.e., the cooperativity reduces in scale with the increasing concentration of doping metal.

Figure 3 shows the plots of a transition width $\Delta T$ vs. $x$ for both $[Fe_{1-x}Zn_x(qnal)_2]\cdot CH_2Cl_2$ and $[Fe_{1-x}Ni_x(qnal)_2]\cdot CH_2Cl_2$ species, where $\Delta T$ is equal to $T$(95%)–$T$(5%), and $T$(95%) and $T$(5%) are temperatures at which $\gamma_{HS}$ equals 95% and 5%, respectively. For zinc(II) and nickel(II) doping, both curves show a upward tendency with increasing $x$ fraction. It reflects that spin transition occurs over larger ranges of temperature as doping is increased. Comparison of curves in Figure 3 reveals no notable difference between the Zn-doping and Ni-doping, suggesting the dominant effect of the doping degree (concentration) rather than metal species on cooperativity.

The evolution of critical temperature $T_{1/2}$ as a function of $x$ fraction is shown in Figure 4, where $T_{1/2}$ is defined as the temperature at $\gamma_{HS}$ equal to 0.5. A noticeable decline is observed in Zn-doping, where the $T_{1/2}$ falls sharply from 217 K ($x = 0$) to 133 K ($x = 0.6$), indicating high dependence of downward shift on the $x$ fraction. However in the case of Ni-doping, a slowdown trend is represented, where $T_{1/2}$ descends slowly to 213 K ($x = 0.6$) as compared with the corresponding value in Zn-doping. The downward shift feature of critical temperature can be explained as a consequence of chemical pressure change in the lattice due to different radii of doping metal ions. Zinc(II) ionic radius (0.74 Å) is closer to that of iron(II) HS (0.78 Å) than that of iron(II) LS (0.61 Å),[29] which favors the construction of host lattice stabilizing iron(II) HS state. On the contrary, the nickel(II) ionic radius (0.69 Å) occupies the size between those of iron(II) HS and LS states.[21] Thus, the effect of internal pressure on iron(II) ions is not prominent in doped lattice, consequently the downward shift of $T_{1/2}$ is not obvious as those observed in Zn-doping. This may reflect that the dependence of the $T_{1/2}$ shift upon $x$ fraction is dominated by internal pressure and associated with the ionic radius of doping metal.

Since the molecular packing of complex **1** shows relatively strong $\pi$–$\pi$ interaction with neighboring molecules, it is reasonable to estimate an effect of the doped site on the occurrence of SCO at the adjacent sites. In order to estimate such an effect, we plotted an SCO fraction $f = \Delta(\chi_m T)/\Delta(\chi_m T)_{x=0}$ as a function of $x$ for mixed-metal systems $[Fe_{1-x}M_x(qnal)_2]\cdot CH_2Cl_2$ (Figure 5), where $\Delta(\chi_m T)$ is defined as $[\chi_m T\ (HT) - \chi_m T\ (LT)]$ at the relevant $x$ fractions and $\Delta(\chi_m T)_{x=0}$ in the case of $x = 0$. Both systems show monotonic decrease of $f$ with increasing $x$. A straight line with a slope of $-1$ represents $f$-values for a model exhibiting no effect on the adjacent sites: only doped sites show no SCO. If the doped site affects the occurrence of SCO at the adjacent sites, the $f$ value should be smaller than the line. In the Zn-doping system, the plots are almost on the line, indicating no effect on $f$ was detected at the neighbors, although another effect on $T_{1/2}$ was detected due to a larger ionic size of zinc(II) (vide supra). However in the Ni-doping system, the plots are a little bit smaller than the expected line, indicating the doped site affects

to some extent the neighbor sites. The magnetic moment residing on nickel(II) ion ($S = 1$) might be the origin of this effect.

## Conclusion

The metal doping increases gradual character and decreases critical temperature $T_{1/2}$ in $[Fe(qnal)_2]\cdot CH_2Cl_2$ complex with a $N_4O_2$ donor set. The cooperativity and $T_{1/2}$ are determined by doping-metal concentration and ionic size, respectively, suggesting a feasible method of modifying spin-transition properties in a certain range by control of the doping degree and doping-metal species. The switch of the dimer combination between the LS and HS states suggests that complex **1** is treatable as a quasi one-dimensional system rather than a dimer and indicates the sensitivity of the crystal lattice to different occupancies of the anti-bonding $e_g$ orbitals on the iron(II) ion accompanying the spin transition between the LS and HS states.

This work was supported in part by a Grant-in-Aid for Science Research from the Ministry of Education, Culture, Sports, Science and Technology, Japan. The authors acknowledge Prof. Osamu Fujino for donation of ICP analysis. The authors are grateful to Kinki University for financial support.

## References

1 L. Cambi, A. Cagnasso, *Atti Accad. Naz. Lincei, Cl. Sci. Fis., Mat. Nat., Rend.* **1931**, *13*, 809.
2 L. Cambi, L. Szego, A. Cagnasso, *Atti Accad. Naz. Lincei, Cl. Sci. Fis., Mat. Nat., Rend.* **1932**, *15*, 266.
3 A. Bousseksou, G. Molnár, G. Matouzenko, *Eur. J. Inorg. Chem.* **2004**, 4353.
4 O. Kahn, C. J. Martinez, *Science* **1998**, *279*, 44.
5 A. B. Gaspar, V. Ksenofontov, M. Seredyuk, P. Gütlich, *Coord. Chem. Rev.* **2005**, *249*, 2661.
6 O. Kahn, J. Kröber, C. Jay, *Adv. Mater.* **1992**, *4*, 718.
7 P. Gütlich, A. Hauser, *Coord. Chem. Rev.* **1990**, *97*, 1.
8 P. Gütlich, Y. Garcia, H. A. Goodwin, *Chem. Soc. Rev.* **2000**, *29*, 419.
9 M. A. Halcrow, *Polyhedron* **2007**, *26*, 3523.
10 D. Boinnard, A. Bousseksou, A. Dworkin, J. M. Savariault, F. Varret, J. P. Tuchagues, *Inorg. Chem.* **1994**, *33*, 271.
11 G. Psomas, N. Bréfuel, F. Dahan, J.-P. Tuchagues, *Inorg. Chem.* **2004**, *43*, 4590.
12 B. Weber, E. Kaps, J. Weigand, C. Carbonera, J.-F. Létard, K. Achterhold, F. G. Parak, *Inorg. Chem.* **2008**, *47*, 487.
13 L. Salmon, A. Bousseksou, B. Donnadieu, J.-P. Tuchagues, *Inorg. Chem.* **2005**, *44*, 1763.
14 V. A. Grillo, L. R. Gahan, G. R. Hanson, R. Stranger, T. W. Hambley, K. S. Murray, B. Moubaraki, J. D. Cashion, *J. Chem. Soc., Dalton Trans.* **1998**, 2341.
15 R. Hernández-Molina, A. Mederos, S. Dominguez, P. Gili, C. Ruiz-Pérez, A. Castiñeiras, X. Solans, F. Lloret, J. A. Real, *Inorg. Chem.* **1998**, *37*, 5102.
16 M. S. Haddad, W. D. Federer, M. W. Lynch, D. N. Hendrickson, *J. Am. Chem. Soc.* **1980**, *102*, 1468.
17 M. S. Haddad, W. D. Federer, M. W. Lynch, D. N. Hendrickson, *Inorg. Chem.* **1981**, *20*, 131.
18 R. Jakobi, H. Spiering, L. Wiehl, E. Gmelin, P. Gütlich, *Inorg. Chem.* **1988**, *27*, 1823.
19 J.-P. Martin, J. Zarembowitch, A. Bousseksou, A. Dworkin, J. G. Haasnoot, F. Varret, *Inorg. Chem.* **1994**, *33*, 6325.
20 J.-P. Martin, J. Zarembowitch, A. Dworkin, J. G. Haasnoot, E. Codjovi, *Inorg. Chem.* **1994**, *33*, 2617.
21 P. Ganguli, P. Gütlich, E. W. Mueller, *Inorg. Chem.* **1982**, *21*, 3429.
22 W. Vreugdenhil, J. G. Haasnoot, O. Kahn, P. Thuery, J. Reedijk, *J. Am. Chem. Soc.* **1987**, *109*, 5272.
23 T. Tayagaki, A. Galet, G. Molnár, M. C. Muñoz, A. Zwick, K. Tanaka, J.-A. Real, A. Bousseksou, *J. Phys. Chem. B* **2005**, *109*, 14859.
24 C. Baldé, C. Desplanches, A. Wattiaux, P. Guionneau, P. Gütlich, J.-F. Létard, *Dalton Trans.* **2008**, 2702.
25 T. Kuroda-Sowa, Z. Yu, Y. Senzaki, K. Sugimoto, M. Maekawa, M. Munakata, S. Hayami, Y. Maeda, *Chem. Lett.* **2008**, *37*, 1216.
26 C. Jiang, J. Wang, F. He, *Anal. Chim. Acta* **2001**, *439*, 307.
27 G. M. Sheldrick, *SHELXS-97, Program for the Solution of Crystal Structures*, University of Göttingen, Germany, **1997**.
28 S. Hayami, Z.-z. Gu, H. Yoshiki, A. Fujishima, O. Sato, *J. Am. Chem. Soc.* **2001**, *123*, 11644.
29 R. D. Shannon, *Acta Crystallogr., Sect. A* **1976**, *32*, 751.